Supporting Information

Flexible Perovskite Solar Cells with Enhanced Performance Based on a Void-Free Imbedded Interface via a Thin Layer of Mesoporous TiO_2

Liangxue Gu[1,2], Haiyan Li[2], Shuiping Gong[2], Xinyu Chen[2], Feng Wen[1] and Songwang Yang[2,3*]*

[1]Special Glass Key Lab of Hainan Province, School of Materials Science and Engineering, Hainan University, Haikou 570228, China. E-mail: fwen323@163.com

[2]CAS Key Laboratory of Materials for Energy Conversion, Shanghai Institute of Ceramics, Chinese Academy of Sciences, 588 Heshuo Road, Shanghai 201899, China. E-mail: swyang@mail.sic.ac.cn

[3]Center of Materials Science and Optoelectronics Engineering, University of Chinese Academy of Sciences, Beijing 100049, China.

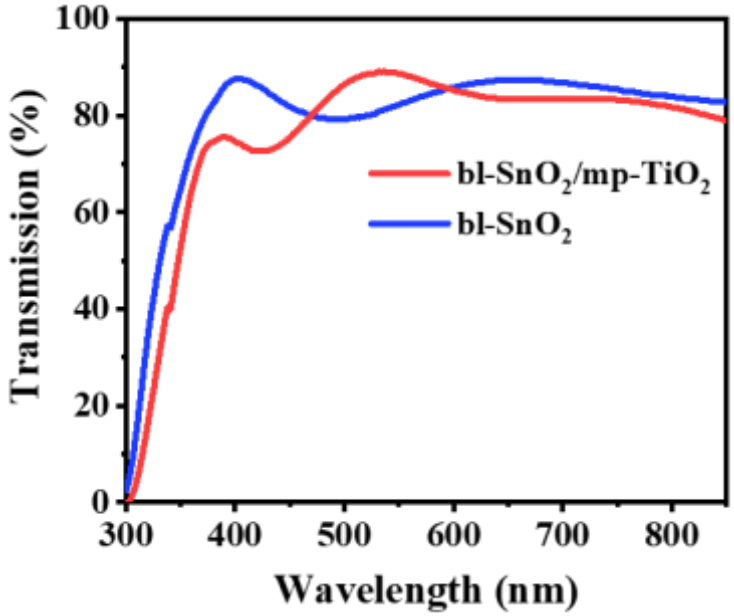

Figure S1. Optical transmission spectra of different ETLs on the ITO glass substrates.

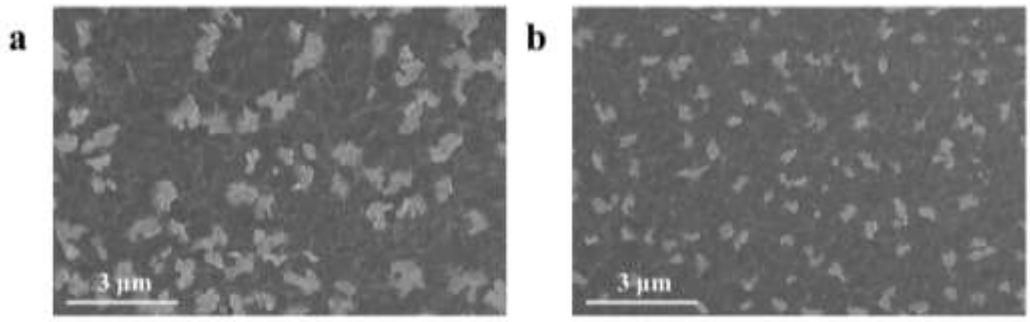

Figure S2. Surface morphologies of perovskite films on (a) bl-SnO_2 and (b) bl-SnO_2/mp-TiO_2 substrates at a low magnification.

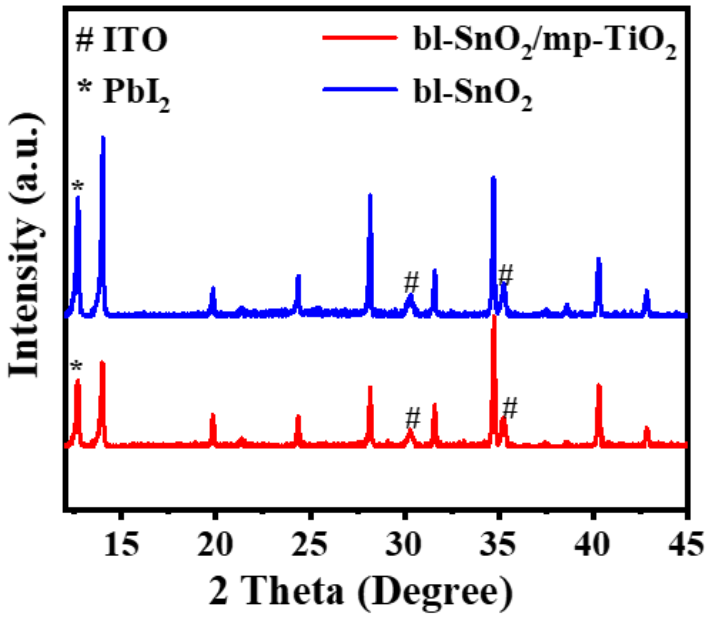

Figure S3. X-ray diffraction patterns of perovskite films based on different ETLs. The main diffraction peaks at around 2θ = 14.0°, 28.2° and 34.7° correspond to (110), (220) and (310) crystal planes, respectively.

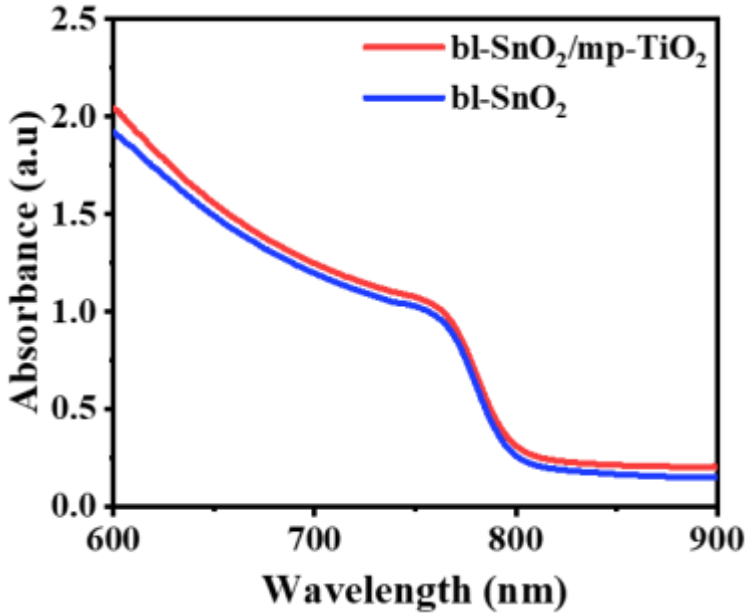

Figure S4. UV-vis absorption spectra of perovskite films on different ETLs.

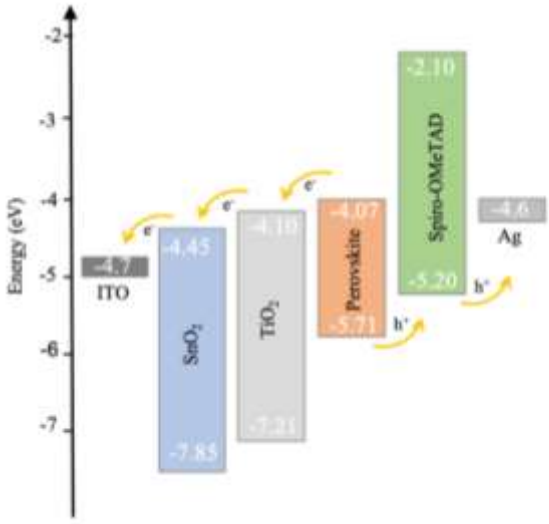

Figure S5. Energy level alignments for the perovskite solar cells based on SnO_2 and TiO_2 composite ETLs.[1-3]

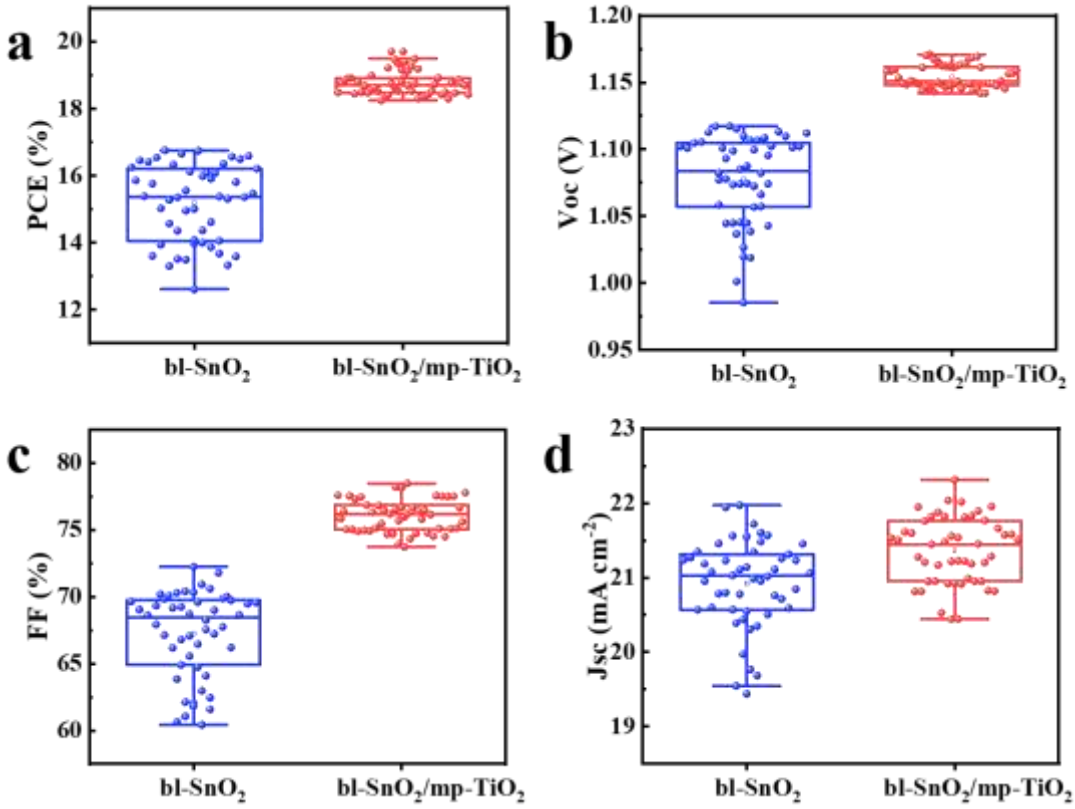

Figure S6. Statistical photovoltaic parameters of devices based on ITO glass substrates. Box plots of the photovoltaic parameters for 50 pieces of devices based on different ETLs. (a) Power conversion efficiency (PCE), (b) open-circuit voltage (Voc), (c) filling factor (FF) and (d) short-circuit current density (Jsc).

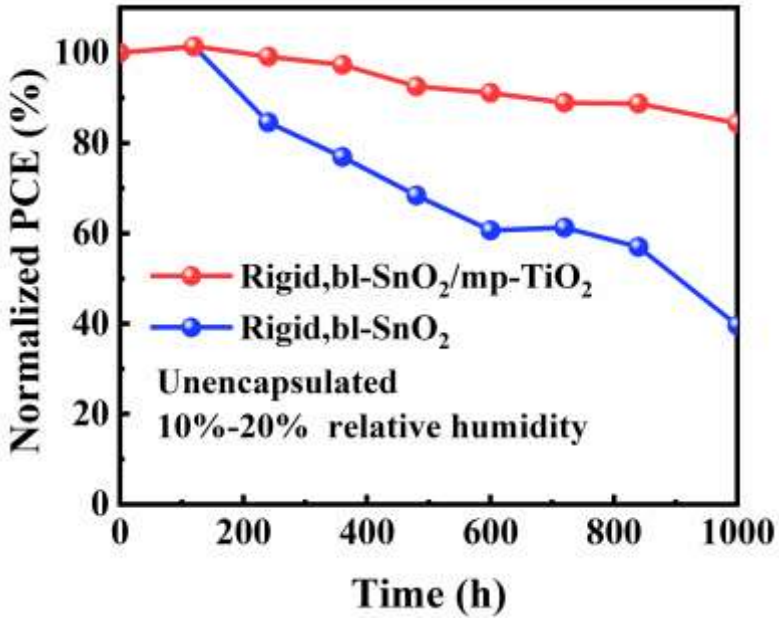

Figure S7. Storage stability of rigid devices based on different ETLs.

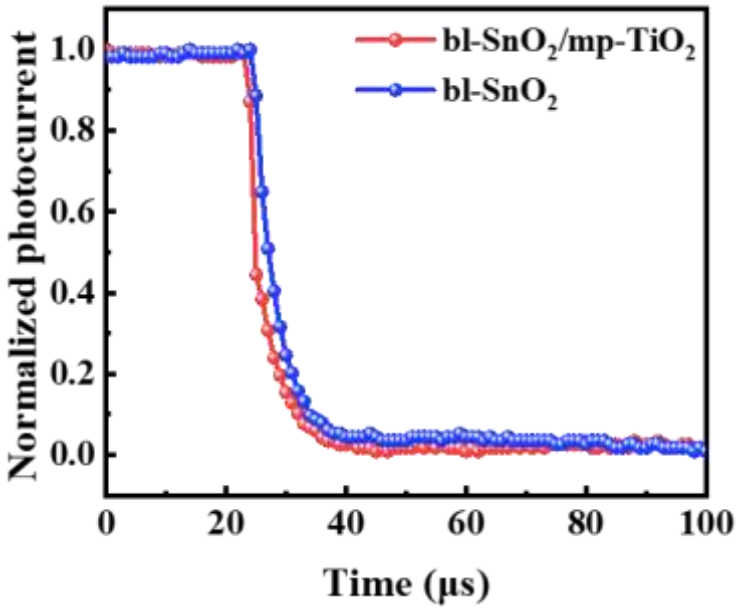

Figure S8. Transient photocurrent (TPC) spectra of devices based on different ETLs (normalized).

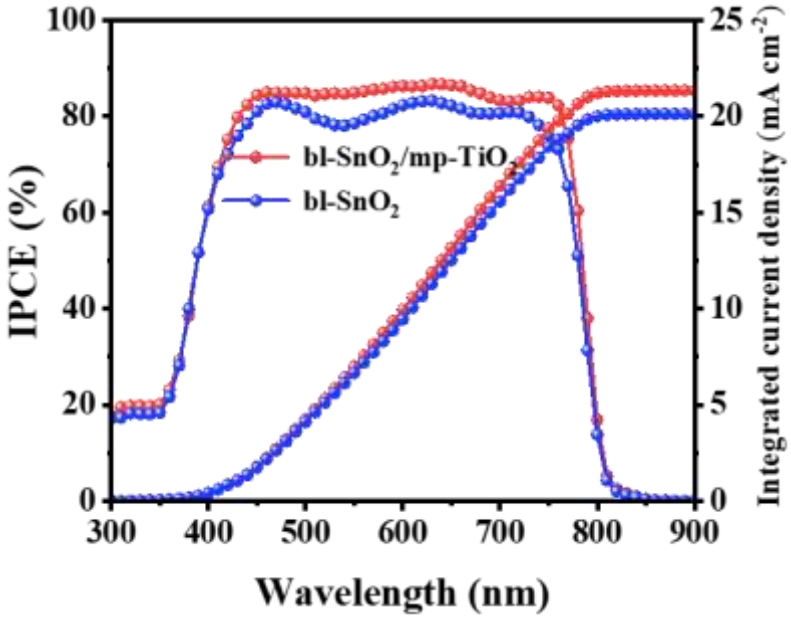

Figure S9. IPCE spectra based on flexible devices with different ETLs.

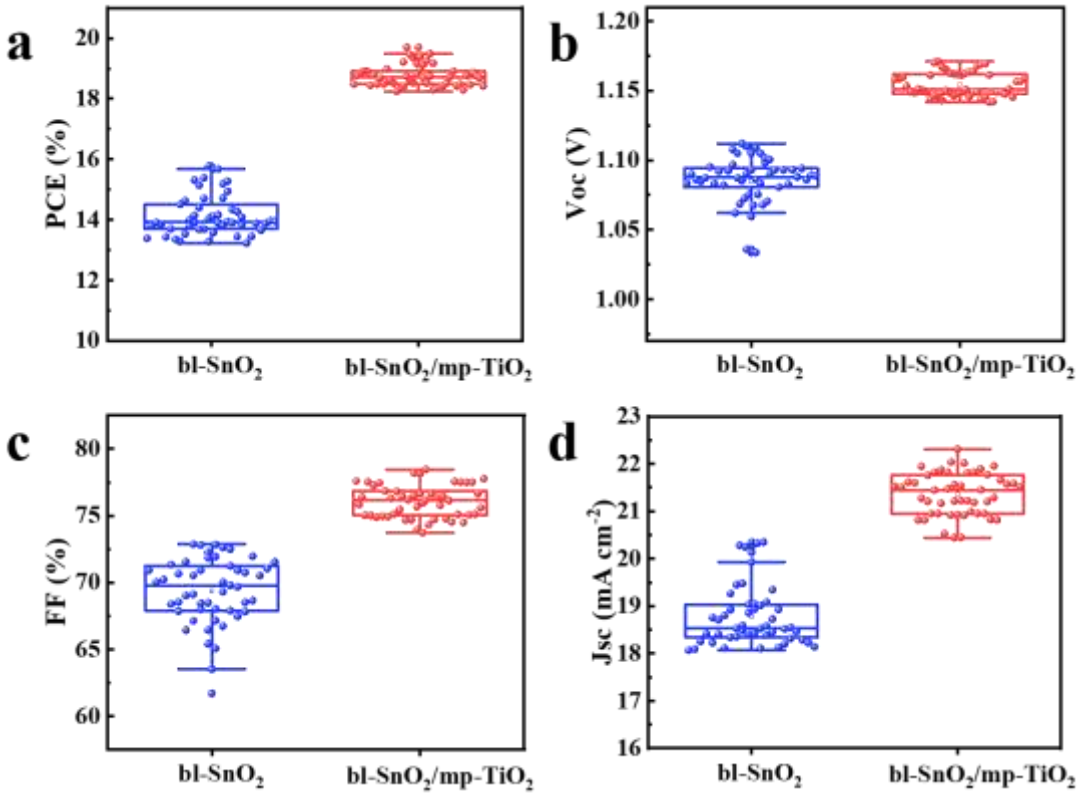

Figure S10. Statistical photovoltaic parameters of devices based on flexible PEN substrates. Box plots of photovoltaic parameters for 50 pieces of samples based on different ETLs, (a) PCE, (b) V_{oc}, (c) FF and (d) J_{sc}.

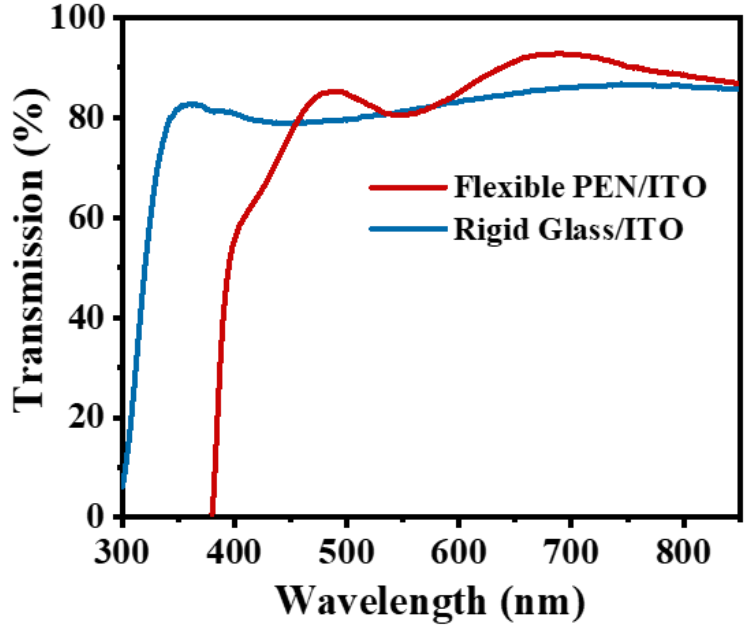

Figure S11. Comparison of the optical transmittance of different substrates.

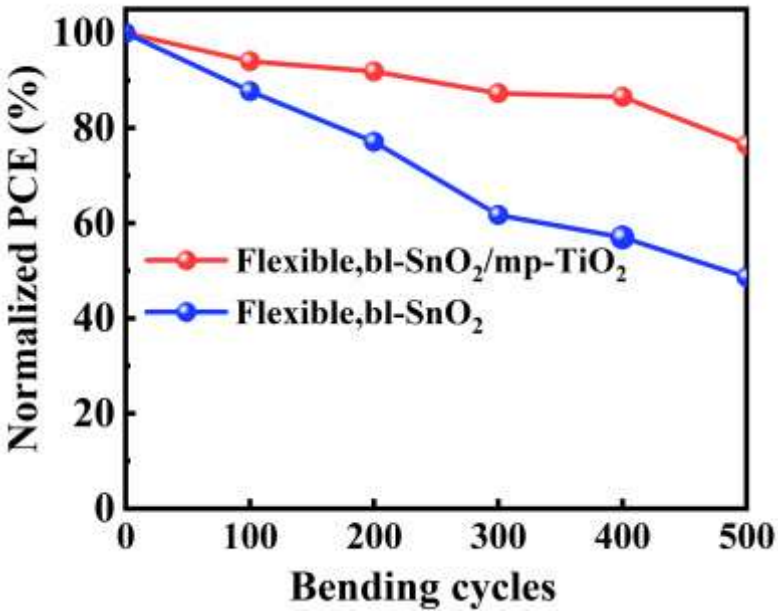

Figure S12. Bending durability of flexible PSCs with 6 mm bending diameter.

Table S1. The average thickness of the ETL layers from the cross-sectional SEM images for the devices and the corresponding calculation results of SCLC measurement.

	Thickness (nm)			V_{TFL} (V)	N_t (cm^{-3})
	ETL	PSK	HTL		
bl-SnO_2	24	486	145	0.64	1.3866×10^{16}
bl-SnO_2/mp-TiO_2	56	587	147	0.27	6.2×10^{15}

Table S2. Average values of photovoltaic parameters for over 50 devices on different substrates, respectively.

Substrate	ETL	V_{oc} (V)	FF (%)	J_{sc} (mA cm^{-2})	PCE (%)	
					Average	Champion
rigid	**bl-SnO_2**	1.07±0.14	67.2±5	20.9±1.4	15.2	16.7
	bl-SnO_2/mp-TiO_2	1.15±0.03	76.0±2.3	21.4±0.9	18.8	19.7
flexible	**bl-SnO_2/mp-TiO_2**	1.16±0.01	75.2±2.1	21.6±0.6	18.7	19.9

Table S3. Fitting results of EIS: series resistance (R_s), transfer resistance (R_{ct}), and recombination resistance (R_{rec}) of devices based on different ETLs.

ETL	R_s (Ω)	R_{ct} (Ω)	R_{rec} (Ω)
bl-SnO_2	37	329	489
bl-SnO_2/mp-TiO_2	18	245	598

Table S4. Summary of devices based on low-temperature TiO_2 ETLs for F-PSCs.

structure	V_{oc} (V)	FF (%)	J_{sc} (mA cm^{-2})	PCE (%)	Source
PEN/ITO/ED-TiO_2/BK-TiO_2/ $MAPbI_3$/spiro/Au	1.07	75	19.51	15.76	Adv. Energy Mater. 2017[4]
PET/ITO/SnO_2/ TiO_2/$FAPbI_3$/ spiro/Au	1.04	66.3	20.9	14.8	Nano Res.2018[5]
PEN/ITO/TiO_2/$FAMAPb(IBr)_3$/ PTAA/Au	0.97	75.6	23.3	17.1	ACS Appl. Mater. Interfaces. 2018[6]
PET/ITO/C_{60}/TiO_x/ $FAMAPb(IBr)_3$/spiro/Au	1.02	71.9	19.63	14.43	J. Mater. Chem. A 2019[7]
PEN/ITO/c-TiO_2/mp-TiO_2/ $MAPbI_3$/spiro/Ag	0.99	74	13.27	9.75	ACS Appl. Mater. 2020 [8]
PEN/ITO/Au-TiO_2/ TiO_2/$FAPbI_3$/spiro/Ag	1.07	64.3	22.29	15.36	ACS Appl. Energy Mater. 2020 [9]
PET/ITO/R-Fu/Lt-TiO_2 / $FAMAPb(IBr)_3$/spiro/Ag	1.05	75	22.93	18.06	Sol. Rrl 2020 [10]
PET/ITO/nano-TiO_2/ $MAPbI_3$/spiro/Au	0.97	67	20.51	13.33	Adv. Mater. 2021 [11]
PEN/ITO/c-TiO_2/mp-TiO_2/ $FAPbI_3$/spiro/Ag	0.99	72.3	20.29	14.52	Appl. Phys. Express. 2021 [12]
PEN/ITO/ TiO_2/ $MAPbI_3$/spiro/Au	1.10	65.6	22.32	16.11	J. Alloy. Compd. 2021[13]
PEN/ITO/SnO_2/TiO_2/$MAPbI_3$/ spiro/Ag	1.16	76.8	22.25	19.9	This work

References

(1) Yi, H.; Wang, D.; Mahmud, M. A.; Haque, F.; Upama, M. B.; Xu, C.; Duan, L.; Uddin, A. Bilayer SnO_2 as Electron Transport Layer for Highly Efficient Perovskite Solar Cells. *ACS Appl. Energy Mater.* **2018**, *1*, 6027-6039.

(2) Kogo, A.; Sanehira, Y.; Numata, Y.; Ikegami, M.; Miyasaka, T. Amorphous Metal Oxide Blocking Layers for Highly Efficient Low-Temperature Brookite TiO_2-Based Perovskite Solar Cells. *ACS Appl. Mater. Interfaces* **2018**, *10*, 2224-2229.

(3) Hu, W.; Zhou, W.; Lei, X.; Zhou, P.; Zhang, M.; Chen, T.; Zeng, H.; Zhu, J.; Dai, S.; Yang, S.; Yang, S. Low-Temperature in Situ Amino Functionalization of TiO_2 Nanoparticles Sharpens Electron Management Achieving over 21% Efficient Planar Perovskite Solar Cells. *Adv. Mater.* **2019**, *31*, 1806095.

(4) Lin, S.-Y.; Su, T.-S.; Hsieh, T.-Y.; Lo, P.-C.; Wei, T.-C. Efficient Plastic Perovskite Solar Cell with a Low-Temperature Processable Electrodeposited TiO_2 Compact Layer and a Brookite TiO_2 Scaffold. *Adv. Energy Mater.* **2017**, *7*, 1700169.

(5) Dagar, J.; Castro-Hermosa, S.; Gasbarri, M.; Palma, A. L.; Cina, L.; Matteocci, F.; Calabro, E.; Di Carlo, A.; Brown, T. M. Efficient Fully Laser-Patterned Flexible Perovskite Modules and Solar Cells Based on Low-Temperature Solution-Processed SnO_2/Mesoporous-TiO_2 Electron Transport Layers. *Nano Res.* **2018**, *11*, 2669-2681.

(6) Wilkes, G. C.; Deng, X. Y.; Choi, J. J.; Gupta, M. C. Laser Annealing of TiO_2 Electron-Transporting Layer in Perovskite Solar Cells. *ACS Appl. Mater. Interfaces* **2018**, *10*, 41312-41317.

(7) Liu, C.; Cai, M. L.; Yang, Y.; Arain, Z.; Ding, Y.; Shi, X. Q.; Shi, P. J.; Ma, S.; Hayat, T.; Alsaedi, A.; Wu, J. H.; Dai, S. Y.; Cao, G. Z. A C-60/TiO_x Bilayer for Conformal Growth of Perovskite Films for UV Stable Perovskite Solar Cells. *J. Mater. Chem. A* **2019**, *7* , 11086-11094.

(8) Nam, J.; Kim, J. H.; Kim, C. S.; Kwon, J. D.; Jo, S. Surface Engineering of Low-Temperature Processed Mesoporous TiO_2 via Oxygen Plasma for Flexible Perovskite Solar Cells. *ACS Appl. Mater. Interfaces* **2020**, *12*, 12648-12655.

(9) Zhao, W.; Yu, M. Y.; Zheng, L. L.; Li, M.; Dai, S. J.; Chen, D. C.; Lee, T. C.; Yun, D. Q. Enhanced Efficiency and Stability of Planar Perovskite Solar Cells Using a Dual Electron Transport Layer of Gold Nanoparticles Embedded in Anatase TiO_2 Films. *Acs Appl. Energy Mater.* **2020**, *3*, 9568-9575.

(10) Wang, P. C.; Govindan, V.; Chiang, C. H.; Wu, C. G. Room-Temperature-Processed Fullerene/TiO_2 Nanocomposite Electron Transporting Layer for High-Efficiency Rigid and Flexible Planar Perovskite Solar Cells. *Sol. RRL* **2020**, *4*, 2000247.
(11) Wu, Z. W.; Li, P.; Zhao, J.; Xiao, T.; Hu, H.; Sun, P.; Wu, Z. H.; Hao, J. H.; Sun, C. L.; Zhang, H. L.; Huang, Z. F.; Zheng, Z. J. Low-Temperature-Deposited TiO_2 Nanopillars for Efficient and Flexible Perovskite Solar Cells. *Adv. Mater. Interfaces* **2021**, *8*, 2001512.
(12) Yin, G. H.; Liu, G.; Ke, L. L.; Rong, M.; Li, H. X. N-Doped Anatase TiO_2 as an Efficient Electron Transport Layer for Mesoporous Perovskite Solar Cells. *Appl. Phys. Express* **2021**, *14*, 076503.
(13) Yang, Z. F.; Chen, W.; Mei, A.; Li, Q. T.; Liu, Y. L. Flexible $MAPbI_3$ Perovskite Solar Cells with the High Efficiency of 16.11% by Low-Temperature Synthesis of Compact Anatase TiO_2 Film. *J. Alloy. Compd.* **2021**, *854*, 155488